Ocean Modelling 111 (2017) 1–8

Contents lists available at ScienceDirect

Ocean Modelling

journal homepage: www.elsevier.com/locate/ocemod

The dependence of the ocean's MOC on mesoscale eddy diffusivities: A model study

John Marshall[a,*], Jeffery R. Scott[a], Anastasia Romanou[b], Maxwell Kelley[b], Anthony Leboissetier[b]

[a] Department of Earth, Atmospheric and Planetary Sciences, Massachusetts Institute of Technology, 77 Massachusetts Avenue, Cambridge, MA 02139-4307, USA

[b] NASA Goddard Institute for Space Studies, 2880 Broadway, New York, NY 10025, USA

ARTICLE INFO

Article history:
Received 20 December 2016
Accepted 14 January 2017
Available online 16 January 2017

Keywords:
Meridional overturning circulation
Mesoscale eddy diffusivity
Global ocean

ABSTRACT

The dependence of the depth and strength of the ocean's global meridional overturning cells (MOC) on the specification of mesoscale eddy diffusivity (K) is explored in two ocean models. The GISS and MIT ocean models are driven by the same prescribed forcing fields, configured in similar ways, spun up to equilibrium for a range of K's and the resulting MOCs mapped and documented. Scaling laws implicit in modern theories of the MOC are used to rationalize the results. In all calculations the K used in the computation of eddy-induced circulation and that used in the representation of eddy stirring along neutral surfaces, is set to the same value but is changed across experiments. We are able to connect changes in the strength and depth of the Atlantic MOC, the southern ocean upwelling MOC, and the deep cell emanating from Antarctica, to changes in K.

1. Introduction

The giant meridional overturning cells of the global ocean (MOC for short) play a central role in setting its structure and are a key agency by which the ocean interacts with the atmosphere above and the cryosphere over the poles. As sketched schematically in Fig. 1, two meridional overturning cells emanate from polar formation regions: (1) an upper cell (of strength Ψ_{NU} in the north and strength Ψ_{SU} in the south) associated with sinking to mid-depth in the northern North Atlantic and upwelling around Antarctica and (2) a lower cell associated with sources of abyssal water around Antarctica (of strength Ψ_{SL}). These cells, and variations thereof, are responsible for meridional and vertical transport of heat, salt (and myriad other quantities) and imprint their signature on key water masses of the global ocean such as North Atlantic Deep Water (NADW) and Antarctic Bottom Water (AABW).

The MOC is a shorthand, zonally-averaged description of an extraordinarily complex 3-dimensional circulation. Its component parts and regional circulations have been studied separately: see, e.g., Marotzke (1997) in the North Atlantic, the upper overturning cell in the SO and its connection to the ACC (Gnanadesikan, 1999; Marshall and Radko, 2003), the deep cell in the SO (Ito and Marshall, 2008) and many other studies. In recent years such regional descriptions have been brought together to investigate how the component parts of the global MOC 'fit together' and interact with one-another: see, e.g., Toggweiler and Samuels (1995); 1998); Gnanadesikan (1999); Wolfe and Cessi (2010); Nikurashin and Vallis (2011); 2012). In these models, upwelling in the SO plays a central role closing the overturning branch of the upper cell, as reviewed in Marshall and Speer (2012).

The traditional view of the global MOC imagined it to be controlled by a vertical 'advective-diffusive balance' (first described by Munk, 1966, in which water sinking at the poles returned through the thermocline: deep waters were assumed to upwell uniformly in the ocean interior, a process balanced by a uniform downward diffusion of heat at a rate set by diapycnal mixing, κ. The strength of the MOC then depends on the diapycnal mixing (scaling suggest a $\kappa^{\frac{2}{3}}$ dependence — see, e.g., Munk and Wunsch, 1998 and the explorations in Mignot et al., 2006 and Kuhlbrodt et al., 2007). Mesoscale eddies play no role in this limit, except in as much as eddies can affect κ by inducing mixing through, for example, lee-wave generation due to the mesoscale interacting with topography (Nikurashin and Ferrari, 2013). Modern descriptions of the upper cell of the MOC, instead, posit an adiabatic return pathway to the surface (Toggweiler and Samuels, 1995; Gnanadesikan, 1999; Marshall and Radko, 2003 and the review by Marshall and Speer, 2012) in which transfer by mesoscale eddies play a central role in connecting the interior to the surface along the slanting

* Corresponding author.
E-mail addresses: jmarsh@mit.edu, marshall@gulf.mit.edu (J. Marshall).

http://dx.doi.org/10.1016/j.ocemod.2017.01.001
1463-5003/

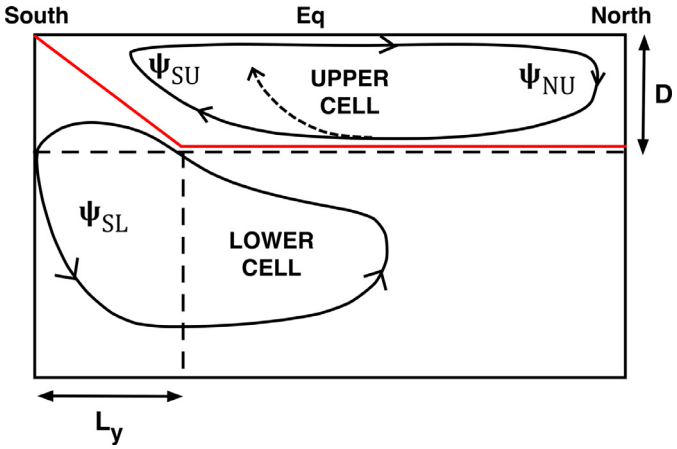

Fig. 1. Schematic diagram of the ocean's meridional overturning circulation. The 'upper cell' emanating from the north has a depth D and strength Ψ_{NU} in the north and Ψ_{SU} in the south. The 'lower cell' emanates from the south and has strength Ψ_{SL} The red line marks the separation between the upper and lower cells and has a slope given by D/L_y imagined to be close to that of isopycnal slopes in the southern ocean in the region of the Antarctic Circumpolar Current. Note that we have also added a diffusive upwelling route through the thermocline indicated by the dotted upward-directed arrow.

isopycnals in the Antarctic Circumpolar Current (ACC) system of the Southern Ocean (SO). If such processes are included in models the strength of the upper cell can become independent of κ. Such possibilities are encoded in to global ocean circulation models through the manner in which the mesoscale eddy field is represented — i.e. in the Gent and McWilliams (1990) parameterization and subsequent developments thereof. In this limit mesoscale eddies play a key role in the dynamics of both the upper cell and the lower cell because they are central to the dynamics of the SO in the region of the tilted red line in Fig. 1.

In summary, then, aside from dependence on external forcing fields such as air-sea momentum and buoyancy fluxes, the processes controlling Ψ have typically been thought about almost exclusively in terms of diapycnal mixing processes, κ. In this paper, instead, we explore the dependence of Ψ on K. We take two coarse-resolution global ocean circulation models configured in a 'realistic domain' with observed bathymetry and coastlines — the GISS ocean model (Schmidt et al. , 2014) and the MITgcm (Marshall et al., 1997a; 1997b) reviewed in the Appendix — and run them out toward equilibrium driven by the same forcing. The models use similar diapycnal mixing schemes (variants on the KPP mixing scheme of Large et al., 1994) and mesoscale eddy closure (but, of course, with respect to the latter, differing numerical implementations thereof). The only parameters that will be varied in the calculations presented here will be the eddy mesoscale diffusivity, K. Our goal will be to study how Ψ_{NU}, Ψ_{SU} and Ψ_{SL} vary with K and use 'modern' theories (e.g. Gnanadesikan, 1999; Marshall and Radko, 2003; Nikurashin and Vallis, 2011; 2012), which take account of the connectedness of these cells and the role of the SO therein, to interpret them. Although only two models are used here, we find that the range of MOC strengths encompassed by them spans the range found in the CORE ocean model intercomparison study (see Danabasoglu et al. , 2014). Thus we believe that the dependencies identified here will have a relevance that transcends the two models used to explore them.

Before going on one should say that there is an appreciation of the importance of K in setting patterns and amplitudes of overturning, particularly among aficionados working in modeling centers. But much of this insight is not written down and, to our knowledge, has not been systematized as we attempt to do here.

Our paper is set out as follows. In Section 2 we describe the experimental design and key properties of the resulting overturning solutions. In Section 3 we consider the upper overturning cell and in Section 4 the lower overturning cell, introducing theory and scaling ideas as needed. In Section 5 we place our study in the context of a wider group of models in which MOCs were compared and contrasted in a model intercomparison study (Danabasoglu et al. , 2014; Farneti et al. , 2015). Finally we discuss and conclude.

2. Experimental design and resulting solutions

2.1. Experiments under CORE-1 protocol

We begin by spinning up our global ocean models toward equilibrium (the MITgcm and GISS ocean model) configured with realistic coastlines and bathymetry at 1° resolution and forced with analyzed fields in a perpetual year. More details of the two models are appended. In our control experiment the mesoscale eddy diffusivity parameter is set equal to a constant $K = 850$ m^{2}s^{-1}, tracers are mixed along neutral surfaces at a rate set by K, and the background diapycnal mixing of the KPP scheme $\kappa = 10^{-5}$ m^{2}s^{-1}. Background diapycnal mixing is kept constant in all our experiments (unless otherwise stated) and only K varied. The CORE1 protocol set out in Griffies et al. (2009) is used as a representation of the forcing. The sea surface salinity is restored in both models on a timescale of 250 days. The models are initialized with the World Ocean Atlas due to Steele et al. (2001), which includes an Arctic analysis, and integrated out for a period of 300 years toward equilibrium. After this time overturning cells are typically within 80–90% of their asymptotic state, sufficient for our current purpose.

Seven experiments are reported here, each carried out with the two models. In five of them the eddy diffusivity was held constant in space and set to $K = 300, 650, 850, 1250$ and 2000 m^{2}s^{-1}. 'Observed' eddy diffusivities vary widely in space in the ocean, as reported, for example, in Abernathey and Marshall (2013). The above Ks roughly span the observed range but do not attempt to capture spatial variations. Two further experiments are also reported. In one K was set to 2000 m^{2}s^{-1} at the surface and prescribed to decay exponentially with an e-folding scale of 600 m, in an attempt to capture the expected surface-intensification of the eddy diffusivity (the 'exp' labels in Figs. 2 and 3) — see Ferreira et al., 2005; Danabasoglu and Marshall, 2007. In our last experiment K was set equal to the aforementioned exponential vertical dependence but the background κ was prescribed to take on a 'Bryan and Lewis' (1979) form in which κ is increased to 10^{-4} m^{2}s^{-1} below 2 km (the 'expbl' label in the figures). This will be of particular interest in our discussion of the deep cell in the SO in section 4. In all experiments the K that is used to stir tracers along neutral surfaces is the same as that used to compute the eddy-induced currents.

2.2. Global overturning cells

Fig. 2 shows the quasi-equilibrium global residual overturning circulation pattern (i.e. Eulerian-mean plus eddy-induced) from GISS (left) and MITgcm (right) as K is varied. We see that both models exhibit an upper cell emanating from the north and a lower from the south. These patterns motivate the schematic, Fig. 1. Note also that both models suggest a rather strong dependence of overturning strengths on K: cell-strengths change by ~40% as K is varied. It is this dependence that is the focus of our attention. These cells play a key role in the uptake of transient tracers and water mass properties, as described in a companion paper, Romanou et al. (2016).

The zonal-average streamfunction shown in Fig. 2 integrates across ocean basins convolving, e.g., the Atlantic and the Pacific.

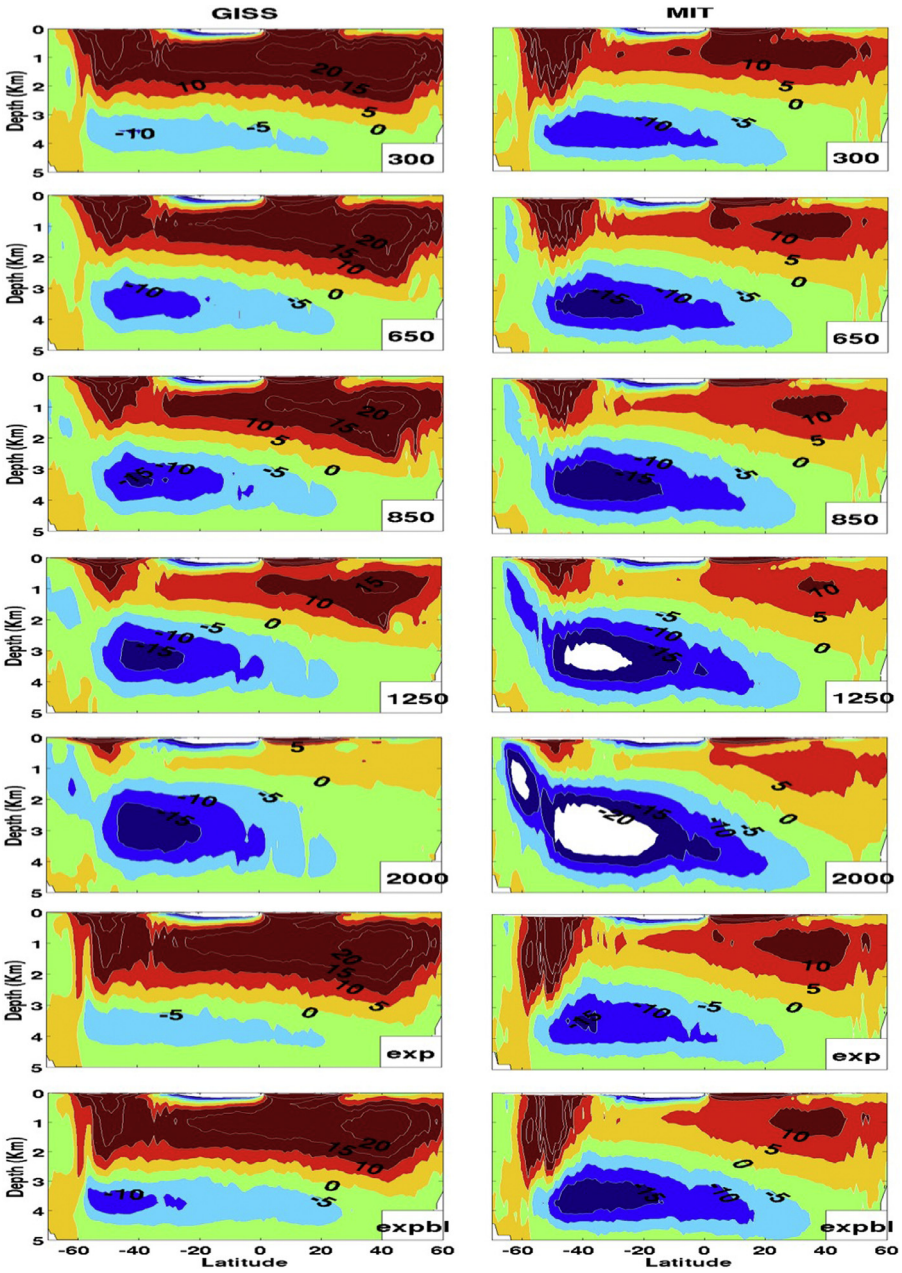

Fig. 2. Global residual overturning streamfunction Ψ_{Global} for the GISS model (left column) and the MIT model (right column) averaged over the last 50 years of a 300 year integration. Contours are plotted with an interval of 5Sv. The particular experiment is denoted by the label on the lower right hand side of each panel.

To isolate the key role of the Atlantic in the northern cell, we now focus on the overturning in the Atlantic sector, the AMOC.

3. Upper cell emanating from the North Atlantic

3.1. Strength and vertical scale of the upper cell

Fig. 3 presents the quasi-equilibrium AMOC streamfunction in the GISS and MIT ocean models across the parameters varied in our suite of experiments. The overturning streamfunctions have a familiar form with downwelling of fluid around 50°N, northward flow near the surface and southward flow at depths around 2km whereby the products of polar convection and mixing are carried away in to the global ocean. The GISS Ψ_{NU} ($\equiv \Psi_{AMOC}$, ranging from 16 $\longrightarrow$ 25 Sv) is considerably stronger and typically extends to greater depths than that of the MITgcm (which ranges from 10$\longrightarrow$15Sv). We also observe that in both models the AMOC strengthens/weakens as it deepens/shallows. We note that the observed AMOC at 26°N has a strength of 18Sv or so and extends to a depth of order 1600 m, as reviewed in Buckley and Marshall (2016). It seems that the GISS model has an AMOC which is typically a little too strong and deep whilst the MIT model has an AMOC which is too weak and shallow. Romanou et al. (2016) compare AMOC strengths in our two models against direct measurements from the RAPID array.

The origin of these systematic differences between the GISS and MIT models cannot be attributed to a single cause. Although the two models are driven by the same CORE-1 forcing and purport to encode the same physical parameterizations, there are many details of implementation which differ. Myriad physical processes play a role in setting overturning strength, most of which are parameterized rather than resolved in our models. Indeed the

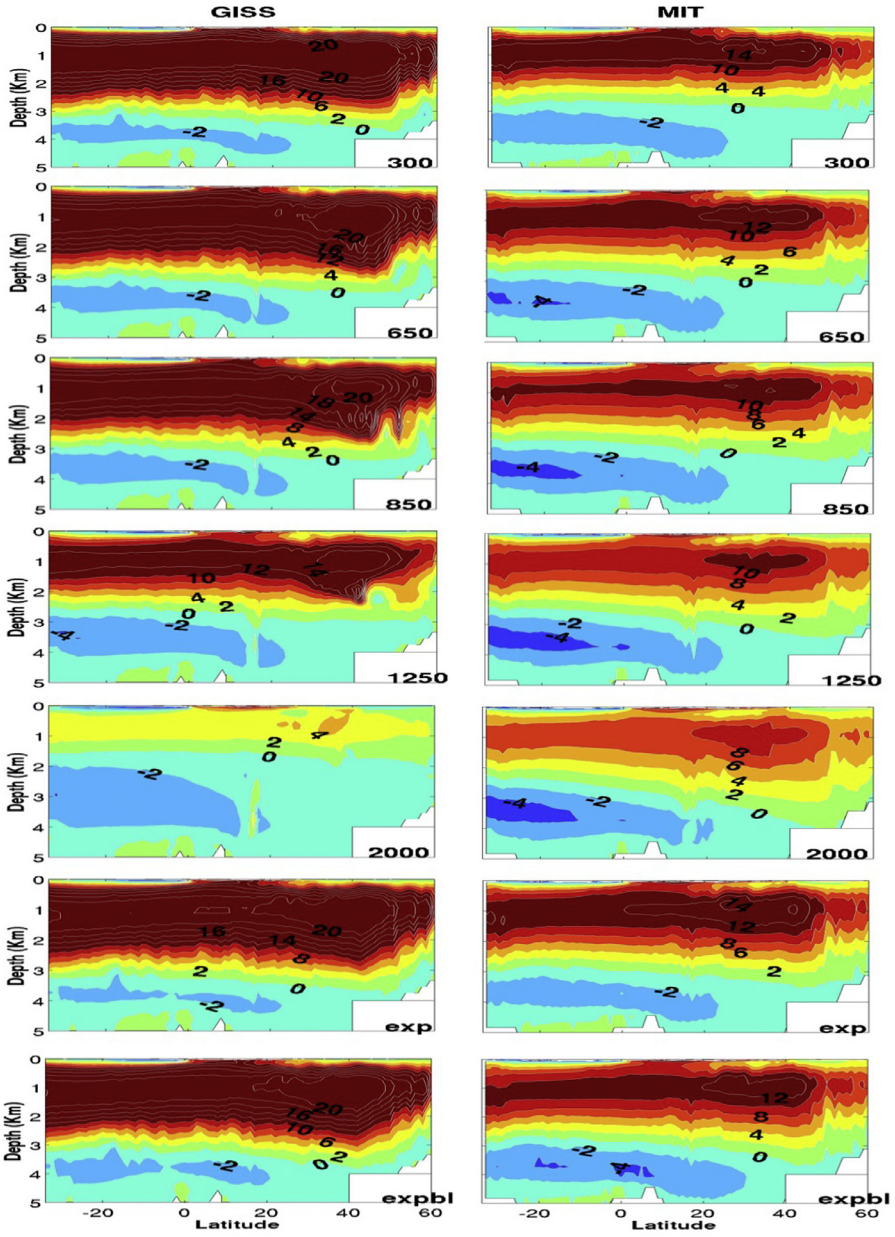

Fig. 3. The residual overturning circulation in the Atlantic sector Ψ_{AMOC} for the GISS model (left column) and the MIT (right column) model, averaged over the last 50 years from 300 year model runs. Contour interval is 2Sv. The particular experiment is denoted by the label on the lower right hand side of each panel.

AMOC is observed to vary widely across ocean models even when they are driven by exactly the same external forcing. As discussed in our concluding remarks, the spread of AMOC amplitudes and depths found by the Danabasoglu et al. (2014) model comparison study is much as observed here.

Despite these differences it should be noted that both GISS and MIT models show *the same* systematic changes in AMOC strength and depth as the mesoscale and diapycnal mixing rates are varied. It is this dependence that is the focus of the present study. To quantify matters we define Ψ_{NU} to be the maximum AMOC streamfunction between 35N and 40N and D to be the average of the depth of the 4-5Sv isolines north of 35S and below a depth of 1000m, similar to that used in Kostov et al. 2014. This criterion for D is used to target the core of southward-flowing NADW, the lower branch of the AMOC. The relationship is summarized in Fig. 4 (top) where Ψ_{NU} and D are plotted against one-another. Both GISS and MIT models in Fig. 4 (top) lie roughly on the same line and span a considerable range of strengths and depths. Such a connection between Ψ_{NU} and D is also found in a wide range of CMIP5 models, as reported in Kostov et al. (2014) and discussed in Section 5. In Fig. 4 (bottom) we plot the % variations of strengths and depths for all our model runs. We see that they exhibit considerable changes — by 30 ⟶ 40% — as parameters are varied.

3.2. Dynamical interpretation

We now attempt to interpret the dependence of Ψ_{NU} on K seen in Figs. 3 and 4 in terms of simple scaling laws. Following Nikurashin and Vallis (2012) we assume that the strength of the northern overturning circulation is proportional to the strength of the zonal geostrophic transport flowing eastward at the margin of the subtropical and subpolar gyres in the North Atlantic. The eastward flow extending to depth D is imagined to be 'converted' in to a meridional overturning cell having the same vertical scale by mixing and convection. The volume transport can be heuristi-

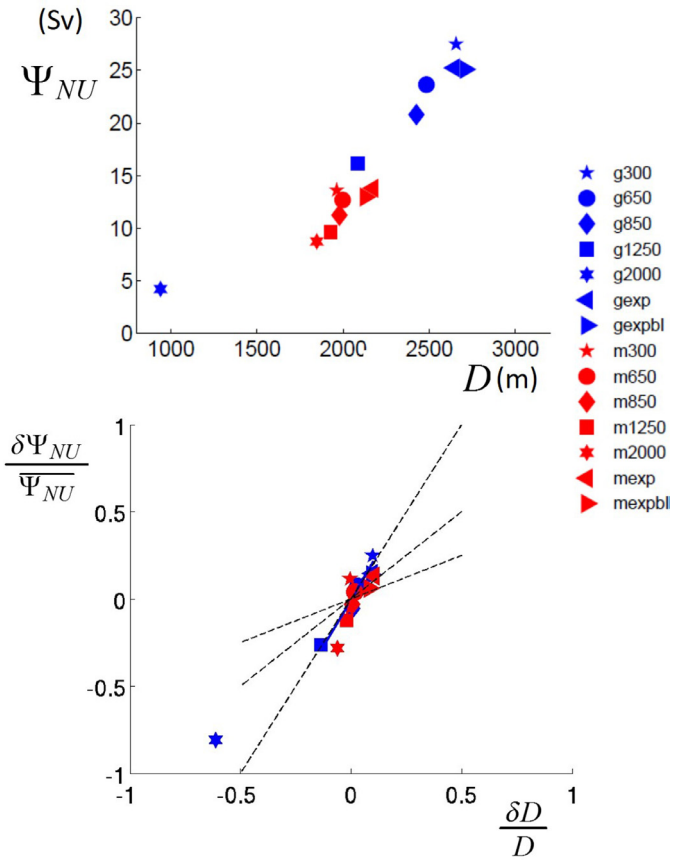

Fig. 4. (a) Strength of AMOC (Ψ_{NU}) vs depth of AMOC (D) from all experiments with the GISS model (blue symbols) and the MIT model (red symbols). (b) Relative change of the strength of the AMOC with the relative change of depth of the AMOC, normalized to the respective experiment means for the GISS and MITgcms. If we fit straight lines to all the runs from each model, the slope of the GISS model fit is 1.4 and for the MIT is 2.1. The dotted lines have slopes of 0.5, 1 and 2.

cally evaluated by vertically-integrating (twice) the thermal wind relation $fu_z = b_y$, where b_y is the meridional buoyancy gradient over the depth D, assumed constant. On so doing we obtain a transport $uD \sim D^2 \frac{b_y}{f}$ suggesting that[1]:

$$\Psi_{NU} = cD^2. \tag{1}$$

Eq. (1) implies that

$$\frac{\delta\Psi_{NU}}{\Psi_{NU}} = 2\frac{\delta D}{D}. \tag{2}$$

In Fig. 4 (top) we plot Ψ_{NU} against D and (bottom) $\frac{\delta\Psi_{NU}}{\Psi_{NU}}$ against $\frac{\delta D}{D}$ where $\overline{\Psi_{NU}}$ is the average across the respective model. In support of the scaling we find that the points lie along a straight line of slope 2. Slope fits are given in the legend. Note that the data point from the GISS model with $K = 2000$ m^{2}s^{-1} is somewhat errant, perhaps due to the collapse of the AMOC at this very high value of eddy diffusivity (see Fig. 3).

Streamlines extending southward at depth emanating from the North Atlantic must 'connect' to the overturning cells in the southern ocean along the red line in the schematic, Fig. 1. Marshall and Speer (2012) review evidence suggesting that this fluid upwells to the surface along sloping neutral surfaces in the southern ocean. This suggests that the strength of the cells in the upper ocean in the N and S are related to one-another. As we now describe, this idea is at the heart of the simple model of thermocline depth and overturning strength proposed by Gnanadesikan (1999).

Adopting the residual-mean theory of the southern ocean developed by Marshall and Radko (2003), we write:

$$\Psi_{SU} = -\frac{\tau}{f} + Ks_\rho = \underbrace{-\frac{\tau}{f}}_{\substack{\text{Eulerian-mean}\\ \overline{\Psi}}} + \underbrace{-K\frac{D}{L_y}}_{\substack{\text{Eddy-induced}\\ \Psi^*}}. \tag{3}$$

where we note that in the southern ocean the isopycnal slope associated with the ACC is negative (slanted red line in Fig. 1) and f is negative.

Taking small variations to express how $\delta\Psi_{SU}$ depends on δK, δD, etc., we have:

$$\delta\Psi_{SU} = -\frac{\delta\tau}{f} - \delta K\frac{D}{L_y} - K\frac{\delta D}{L_y}$$

where we assume that L_y does not change. The latter assumption is reasonable since L_y is likely largely set by geometry (bathymetry and Drake Passage) but is relaxed by Wolfe and Cessi (2014) in a study of salt feedbacks on the overturning circulation.

We now suppose that changes in the southern overturning strength $\delta\Psi_{SU}$ are reflected in changes in $\delta\Psi_{NU}$: setting $\delta\Psi_{SU} = \delta\Psi_{NU}$ and making use of Eq. (2) we arrive at:

$$\frac{\delta D}{D}\left(1 + 2\frac{\Psi_{NU}}{|\Psi^*|}\right) + \frac{\delta K}{K} + \frac{\delta\tau}{f}\left(\frac{1}{|\Psi^*|}\right) = 0 \tag{4}$$

and $|\Psi^*| = K\frac{D}{L_y}$ is the strength of the eddy-induced circulation contribution to Ψ_{SU}.

In our CORE-1 calculations the wind does not change across solutions and so, setting $\delta\tau = 0$ we find:

$$\frac{\delta D}{D} = -\frac{1}{\left(1 + 2\frac{\Psi_{NU}}{\Psi^*}\right)}\frac{\delta K}{K}.$$

This yields, from Eq. (2), the following prediction for the dependence of changes in upper cell strength in the north on changes in K:

$$\frac{\delta\Psi_{NU}}{\Psi_{NU}} = -\frac{2}{\left(1 + 2\frac{\Psi_{NU}}{\Psi^*}\right)}\frac{\delta K}{K}. \tag{5}$$

Thus we expect Ψ_{NU} to decrease as K increases, as indeed is observed in Fig. 3.

Fig. 5 (top) plots $\delta\Psi_{NU}$ against $\delta\Psi_{SU}$, normalized against their respective means. The strength of the upper overturning cell, Ψ_{SU}, is defined here as the average of the residual overturning strength in the upper 2km of the ocean (for $\Psi_{SU} > 0$) between 40°S and 60°S. We see that cell strengths in the two models lie along respective lines, but that the GISS model is somewhat closer to a line of slope unity. It is clear from inspection of Fig. 2 that the GISS model typically has stronger, deeper upper overturning cells which more directly connect between the hemispheres. Thus changes in the strength of one cell is reflected in the other. The MIT model, on the other hand, has a weaker upper cell which, as the eddy diffusivity is increased, becomes less contiguous across the equator perhaps leading to a breakdown of our scaling which relies on interhemispheric connectivity between Ψ_{NU} and Ψ_{SU}. This may be due to enhanced diapycnal mixing processes in MITgcm compared to GISS which can break the connection between the transports of the northern and southern cells, as indicated by

[1] It is interesting to note that the model of Gnanadesikan (1999) implicitly assumes the same scaling law, but arrived at in a subtly different way and with a different interpretation of D. Gnanadesikan assumes that Ψ_{NU} scales as the *northward* geostrophic transport of upper-layer fluid integrated across the basin. The same D^2 dependence is found but D must now be interpreted as the depth above which geostrophic transport is directed northward. Here, instead, D is the full depth of the overturning cell.

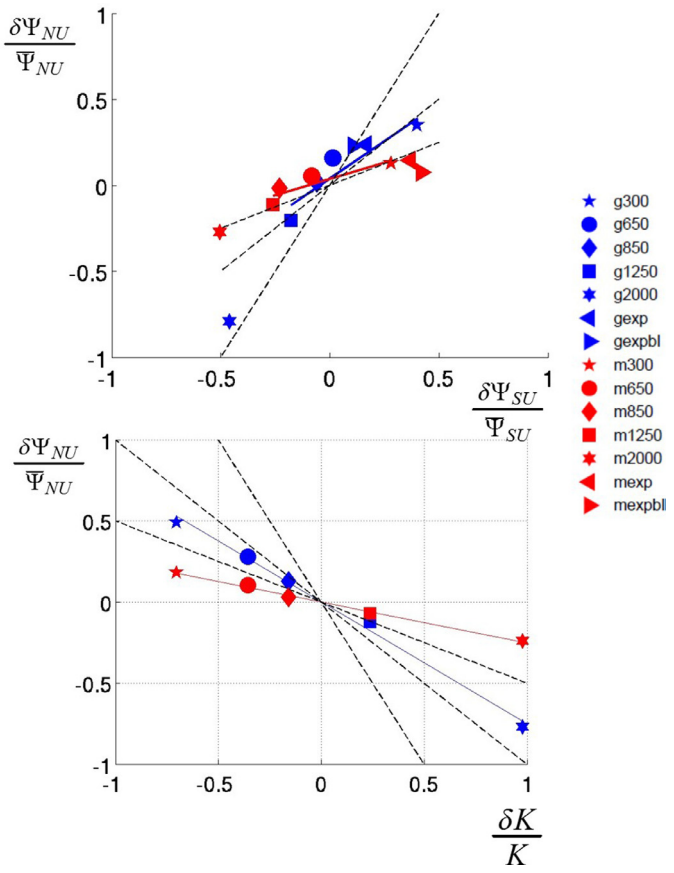

Fig. 5. (a) Change of strength of AMOC with change of strength in the Southern Ocean upper cell. The fits are computed based on all 7 runs for each model and the slopes are 1.3 for GISS and 0.5 for MIT. The strength of the AMOC is computed as before, the strength of Ψ_{SU} is computed as the mean of the residual overturning in the upper 2km of the ocean. Dotted lines have slopes of 0.5, 1 and 2. (b) Change in the strength of AMOC with change in mesoscale diffusivity. The fit is computed on the 5 runs with constant diffusivities: the slope for GISS is −0.75 and for MITgcm −0.2. Dotted lines have slopes of −0.5, −1 and −2.

the dotted arrow in the upper cell of Fig. 1. For simplicity our analysis assumes the 'weak mixing' limit of Nikurashin and Vallis whereas diapycnal mixing processes (explicit or implicit in the model numerics) may need to be included for a more complete description. This question is left open for further work.

Fig. 5 (bottom) plots the dependence of $\delta\Psi_{NU}$ on δK, excluding runs in which K decayed with depth. Typically, we find that $\frac{\Psi_{NU}}{\Psi^*}$ is order 2 and so Eq. (5) suggests that the points ought to cluster around a line with a negative slope of 0.4. Pleasingly, as can be seen in Fig. 5, both models are broadly in accord.

The control on the strength of the AMOC in the north is a consequence of changes in the dynamics of its upwelling branch*in the south*. An increase in K results in the wind-driven Deacon Cell, $\overline{\Psi}$ in Eq. (3), being more completely compensated by Ψ^* resulting in a weakening of the residual-mean circulation Ψ_{SU}. On long time-scales, and in the time-mean considered here, by volume conservation this weakening is also manifest in the downwelling branch of the AMOC. This occurs even though the local contribution of Ψ^* to Ψ_{NU} is small relative to the Eulerian-mean. It should be noted, however, one might not always expect to see a very tight connection between $\delta\Psi_{NU}$ and $\delta\Psi_{SU}$. In observations, as indeed in models, there is considerable exchange between the upper and lower cells. As emphasized by Talley et al. (2003) and reviewed in Marshall and Speer (2012), in the present climate perhaps as much as 75% of the NADW flowing southward in to the SO sinks to ventilate the lower cell: it does not all feed the upper cell. Nevertheless, although one might not expect $\delta\Psi_{NU} = \delta\Psi_{SU}$ (due to 'leakage') as assumed in deriving Eq. (4), it is not surprising that they covary with one-another as seen in Fig. 5a. This will be checked in a wider spectrum of models in Section 5.

4. Lower cell emanating from the southern ocean

4.1. Strength and vertical scale of the lower cell

The abyss is largely ventilated by the lower cell of the MOC fed from the south in processes associated with the formation of AABW, as indicated by Ψ_{SL} in Fig. 1. Unlike Ψ_{SU}, the dynamics of Ψ_{SL} is not as directly tied to the wind field but depends on mixing/convective and eddy processes around Antarctica. Plots of the global overturning circulation, Ψ_{Global}, from our two models can be seen in Fig. 2: the lower cell is evident as the blue clockwise cell in the abyssal southern ocean. It exhibits a clear dependence on the K, becoming stronger as K increases, in contrast to the AMOC which weakens. But it is clear that Ψ_{SL} must also be associated with diapycnal mixing processes which allow AABW to rise in the water column from the abyss up to mid-depth. From there it can be swept quasi-adiabatically along tilted neutral surfaces up to the surface upwelling around Antarctica. Indeed, by comparing the bottom two panels of Fig. 2 in which the K 's are the same, we see that Ψ_{SL} increases when the Bryan and Lewis (1979) scheme is employed, which augments κ in the abyssal ocean.

As can be seen in Fig. 6 (top) the strength and vertical extent of the lower cell change in a systematic way as parameters are varied in both the GISS and MIT models. Note that because the lower cell is clockwise, Ψ_{SL} is negative, but in Fig. 6 $|\Psi_{SL}|$ is plotted. The strength of the lower cell is computed as $|\Psi_{SL}|$ below 2000m and between 60S and 20S. The extent of the lower cell is computed as the average depth of the 0 and lower −5 SV contours, north of 60S and south of 20S. In both the GISS and MIT models, $|\Psi_{SL}|$ increases as K and k are increased and D_{Lower} increases as $|\Psi_{SL}|$ increases: the stronger the deep cell becomes the greater is its vertical extent. It should also be mentioned that as the lower cell strengthens and expands vertically it also extends further equatorwards.

4.2. Dynamical interpretation

We follow the scaling ideas of Ito and Marshall (2008) who invoke diapycnal mixing to balance cross-isopycnal mass flux by the residual-mean flow of the lower cell. These ideas are also encapsulated in the Nikurashin and Vallis (2012) model. Integrating the buoyancy balance over the abyssal layer they obtain a diagnostic relationship, $\Psi_{SL}s_\rho \propto \kappa$, indicating that the product of the lower-limb circulation and the isopycnal slope is proportional to the diapycnal diffusivity. Physically, this relationship indicates that the overturning circulation must balance buoyancy forcing due to diapycnal mixing, and the intensity of Ψ_{SL} is proportional to κ if the isopycnal slope s_ρ is prescribed. In reality, changes in κ also impact the buoyancy structure and so the variation of s_ρ also needs to be taken in to account. Ito and Marshall show that in their idealized numerical experiments, the lower-limb circulation is primarily associated with the eddy-induced circulation, $\Psi_{SL} \sim \Psi^* \sim Ks_\rho$. Combining with $\Psi_{SL}s_\rho \propto \kappa$, the key scaling relation of the Ito and Marshall study emerges for the intensity of the lower limb: $\Psi_{SL} \propto \sqrt{\kappa K}$. Thus we expect:

$$\frac{\delta\Psi_{SL}}{\overline{\Psi}_{SL}} = \frac{1}{2}\frac{\delta K}{K} \tag{6}$$

We now use this as a simple framework from which to interpret the results of our numerical experiments.

In Fig. 6 (bottom) we plot $\frac{\delta\Psi_{SL}}{\overline{\Psi}_{SL}}$ against $\frac{\delta K}{K}$ for both GISS and MITgcm. Pleasingly, we see that the points from lie along a line

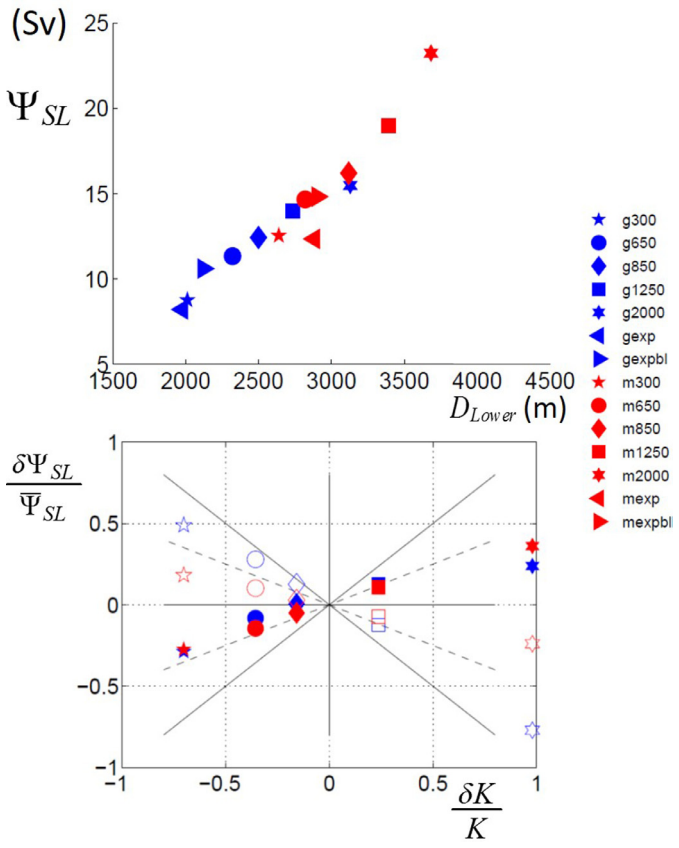

Fig. 6. (a) Strength of the lower cell plotted against its upward vertical extent measured from the bottom. Means of the last 50 years are taken from each run. (b) Relative change of the strength of the upper and lower cells with the relative change of mesoscale diffusivity in the GISS (blue symbols) and the MIT models (red symbols). Upper cell is indicated with the hollow symbols: lower cell with the full symbols. Only the constant coefficient K experiments are shown. The $\pm$ 1 and $\pm$ 0.5 lines are also shown with continuous and dashed black lines respectively. Horizontal axis: $\delta K/K$.

which has a slope or roughly 1/2, as would be expected if Eq. (6) is obeyed. It should also be noted that Ψ_{SL} increases in both models when the abyssal diapycnal mixing rates are increased, as in the Bryan and Lewis (1979) implementation.

5. Conclusions

We have studied the strength and depth of the ocean's upper and lower global residual overturning cells and their dependence on mesoscale eddy diffusivity in the GISS and MITgcms. A recurring theme of the study has been that although mesoscale eddy effects are only important locally in special regions of the global ocean, such as the ACC where Ψ^* and $\overline{\Psi}$ in Eq. (3) are of comparable magnitude, they have global import because of the central role of the SO in interhemispheric overturning dynamics (Marshall and Speer, 2012). Scaling laws implicit in the work of Gnanadesikan (1999); Marshall and Radko (2003); Ito and Marshall (2008) and Nikurashin and Vallis (2011, 2012), have enabled us to rationalize the dependence found in the two models.

In Fig. 7 we illustrate how the framework set out here may be useful in the interpretation of the overturning cells in a wider range of models. Fig. 7a shows Ψ_{NU} plotted against D across a further 9 z-coordinate models that were part of the model comparison described in Danabasoglu et al. (2014) and Farneti et al. (2015). Note that the strengths of the AMOC varies between 10 to 28Sv with depths of 2–3 km or so. The GISS and

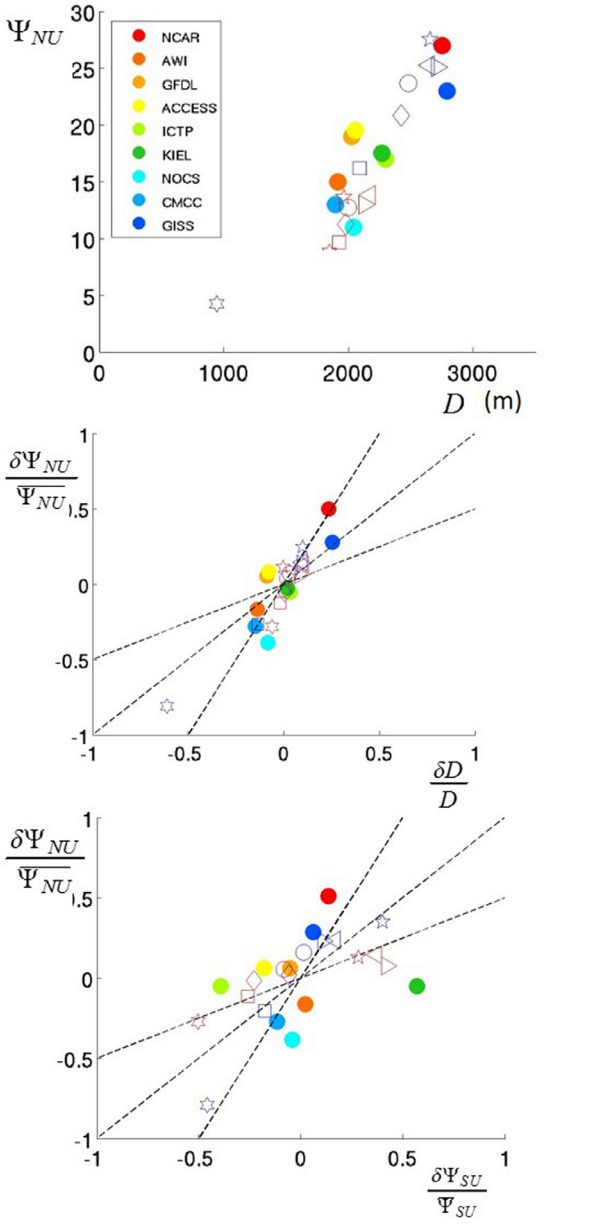

Fig. 7. (a) AMOC max from Danabasoglu et al. (2014) plotted against D, the depth of the 5Sv contour across CORE2 models, as in Fig. 4a. (b) Relative change of the strength of the AMOC with the relative change of depth of the AMOC, normalized to the respective experiment across the CORE2 models, as in Fig. 4b. (c) Relative change of strength of AMOC plotted against the relative change of strength in the Southern Ocean upper cell, computed as in Fig. 5, but for the CORE2 models from Farneti et al. (2015). For comparison, the open (ghost) symbols plot the corresponding data from the GISS and MIT models. Lines of slope 0.5, 1 and 2 are plotted in (a) and (b).

MIT models explored in this paper span roughly the same range and are also plotted in the figure as the hollow 'ghost' points for reference. Moreover, as can be seen in Fig. 7b relation (2) is obeyed with the models scattered around a line of slope 2: the stronger the AMOC the greater is its vertical extent. Fig. 7c shows that there is a connection between the strengths of the upper and lower cells in the north and the south across the CORE models, demonstrating the global 'connectivity' of the overturning cells. An important consequence is that model choices made with respect to processes in the south will have implications for the overturning strength and depth in the north, and visa-versa.

Finally, we return to the question of why the GISS and MIT ocean models exhibit rather different absolute overturning

strengths despite purporting to encode the same 'dynamics' and 'physics'. It is clear that the AMOC is not a robust emergent property of our models, unlike, for example, Sverdrup balance or Ekman layer transport. Instead it is a 2-d, zonally-averaged compression of a very complex 3-d circulation. Myriad physical processes are at work, many of which are parameterized rather than resolved in our models such as: mesoscale tapering schemes, implementation of residual-mean representation of mesoscale eddy fluxes, advection schemes, resolution both in the vertical and the horizontal, bathymetry, mixing schemes, representation of overflows etc. Despite the sensitivity of the mean state to details of model implementation, it is gratifying to report that the dependence of $\delta\Psi$ on δK can be rationalized through scaling laws motivated by our understanding of key underlying mechanisms and interactions between Ψ_{NU}, Ψ_{SU} and Ψ_{SL}. These same processes are at work across a much wider range of models, as illustrated in Fig. 7.

Acknowledgments

Resources supporting this work were provided by the NASA 368 High-End Computing (HEC) Program through the NASA Center for Climate Simulation 369 (NCCS) at Goddard Space Flight Center. Funding was provided by NASA-ROSES Modeling, Analysis and Prediction 2009 NNH10ZDA001N-MAP. We especially thank Gary Russell for his continuous support of the NASA Ocean Modeling work and Lilly Del Valle at NASA-GISS for graphics design support. J.S. received support from the Joint Program on the Science and Policy of Global Change, which is funded by a number of federal agencies and a consortium of 40 industrial and foundation sponsors.

Appendix

Both the GISS and MITgcm models used in this study were configured with realistic bathymetry at a nominal 1° resolution and forced with CORE-1 fields in a perpetual year, as described in Griffies et al. (2009). Both employed the KPP mixing scheme (Large et al., 1994) with a background diapycnal mixing of 10^{-5} $m^2\,s^{-1}$ along with a Gent and McWilliams (1990) eddy parameterization based on 'residual-mean theory'. In particular an extra advection term has been added to the Eulerian mean to represent 'quasi-Stokes' advection by eddies (McDougall and McIntosh, 1996). The eddy advection is parameterized in terms of mean flow quantities through an eddy diffusivity K. This same eddy diffusivity is used to mix tracers along isoneutral surfaces. Both models employed the Prather advection scheme for heat, salt, and tracers.

The MITgcm (Marshall et al., 1997a; 1997b) was run with 50 vertical levels and a hybrid latitude-longitude and cubed-sphere horizontal grid as described in Forget et al. (2015). More details of the equilibrium solution with a reference $K = 850$ $m^2\ s^{-1}$ can be found in Marshall et al. (2015).

The GISS ocean model was run in its 32-level longitude-latitude configuration whose climatology when coupled to the GISS atmosphere model was described by Schmidt et al. (2014). Differences relative to that version include the aforementioned choices for tracer advection scheme and mesoscale diffusivity K, a correction to the mesoscale scheme to correctly orient transports along isoneutral surfaces, and improvements to the sea ice component.

References

Abernathey, R.P., Marshall, J., 2013. Global surface eddy diffusivities derived from satellite altimetry. J. Geophys. Res. Vol. 118 (2), 901–916.
Bryan, K., Lewis, L., 1979. A water mass model of the world ocean. J. Geophys. Res. 84, 2503–2517.
Buckley, M.W., Marshall, J., 2016. Observations, inferences, and mechanisms of atlantic meridional overturning circulation variability: a review. Rev. Geophys. 54. doi:10.1002/2015RG000493.
Danabasoglu, G., Marshall, J., 2007. Effects of vertical variations of thickness diffusivity in an ocean general circulation model. Ocean Model. vol. 18 (no. 2), 122–141.
Danabasoglu, G., et al., 2014. North atlantic simulations in coordinated ocean-ice reference experiments phase II (CORE-II). Part I: Mean states Ocean Model. Vol 73, 76–107.
Farneti, et al., 2015. An assessment of antarctic circumpolar current and southern ocean meridional overturning circulation during 1958–2007 in a suite of interannual CORE-II simulations. Ocean Model. 93, 84–120.
Ferreira, D., Marshall, J., Heimbach, P., 2005. Estimating eddy stresses by fitting dynamics to observations using a residual-mean ocean circulation model and its adjoint. J. Phys. Oceanogr. vol. 35 (no. 10), 1891–1910.
Forget, G., Campin, J.-M., Heimbach, P., Hill, C.N., Ponte, R.M., Wunsch, C., 2015. ECCO Version 4: an integrated framework for non-linear inverse modeling and global ocean state estimation. Geosci. Model Dev. 8 (no. 10), 3071–3104.
Gent, P.R., McWilliams, J.C., 1990. Isopycnal mixing in ocean circulation models. J. Phys. Oceanogr. 20, 150–155.
Gnanadesikan, S., 1999. A simple predictive model for the structure of the oceanic pycnocline. Science 283, 2077–2079.
Griffies, S., Biastoch, A., Böning, C., Bryan, F., Danabasoglu, G., Chassignet, E.P., England, M.H., Gerdes, R., Haak, H., Hallberg, R.W., Hazeleger, W., Jungclaus, J., Large, W.G., Madec, G., Pirani, A., Samuels, B.L., Scheinert, M., Gupta, A.S., Severijns, C.A., Simmons, H.L., Treguier, A.M., Winton, M., Yeager, S., Yin, J., 2009. Coordinated ocean-ice reference experiments (COREs). Ocean Model 26, 1–46.
Ito, T., Marshall, J., 2008. Control of lower-limb overturning circulation in the southern ocean by diapycnal mixing and mesoscale eddy transfer. J. Phys. Oceanogr. 38, 2832–2845. http://dx.doi.org/10.1175/2008JPO3878.1.
Kostov, Y., Armour, K.C., Marshall, J., 2014. Impact of the atlantic meridional overturning circulation on ocean heat storage and transient climate change. Geo. Res. Lett. Volume 41 (Issue 6), 2108–2116.
Kuhlbrodt, T., Griesel, A., Montoya, M., Levermann, A., Hofmann, M., Rahmstorf, S., 2007. On the driving processes of the atlantic meridional overturning circulation. Rev. Geophys. 45, RG2001. doi:10.1029/2004RG000166.
Large, W., McWilliams, J., Doney, S., 1994. Oceanic vertical mixing: a review and a model with nonlocal boundary layer parameterization. Rev. Geophys. 32, 363–403.
Marotzke, J., 1997. Boundary mixing and the dynamics of three-dimensional thermohaline circulations. J. Phys. Oceanogr. 27, 1713–1728.
Marshall, J., Adcroft, A., Hill, C., Perelman, L., Heisey, C., 1997a. A finitevolume, incompressible navier stokes model for studies of the ocean on parallel computers. JGR Oceans 102 (C3), 5753–5766.
Marshall, J., Hill, C., Perelman, L., Adcroft, A., 1997b. Hydrostatic, quasihydrostatic, and nonhydrostatic ocean modeling. JGR Oceans 102 (C3), 5733–5752.
Marshall, J., Radko, T., 2003. Residual mean solutions for the antarctic circumpolar current and its associated overturning circulation. J. Phys. Oceanogr. 33, 2341–2354.
Marshall, J., Scott, J.R., Armour, K.C., Campin, J.-M., Kelley, M., Romanou, A., 2015. The ocean's role in the transient response of climate to abrupt greenhouse gas forcing. Clim. Dyn. 44 (7), 2287–2299.
Marshall, J., Speer, K., 2012. Closure of the meridional overturning circulation through southern ocean upwelling. Nat. Geosci. 5 (3), 171–180.
McDougall, T.J., McIntosh, P.C., 1996. The temporal-residual-mean velocity. part i: derivation and the scalar conservation equations. J. Phys. Oceanogr. 26, 2653–2665.
Mignot, J., Levermann, A., Griesel, A., 2006. A decomposition of the atlantic meridional overturning circulation into physical components using its sensitivity to vertical diffusivity. J. Phys. Oceanogr. vol 36, 636–650.
Munk, W., 1966. Abyssal recipes. Deep-Sea Res. 13, 707–730.
Munk, W., Wunsch, C., 1998. Abyssal recipes II Energetics of the tides and wind. Deep-Sea Res. 45, 1976–2009.
Nikurashin, M., Ferrari, R., 2013. Overturning circulation driven by breaking internal waves in the deep ocean. Geophys. Res. Lett. 40, 3133–3137.
Nikurashin, M., Vallis, G., 2011. A theory of deep stratification and overturning circulation of the ocean. J. Phys. Oceanogr. 41, 485–502.
Nikurashin, M., Vallis, G., 2012. A theory of the interhemispheric meridional overturning circulation and associated stratification. J. Phys. Oceanogr. 42, 1652–1667. http://dx.doi.org/10.1175/JPO-D-11-0189.1.
Romanou, A., Marshall, J., Kelley, M., Scott, J., 2016. Role of the ocean's AMOC in the uptake of transient tracers. Submitted to GRL.
Schmidt, G.A., et al., 2014. Configuration and assessment of the GISSModele2 contributions to theCMIP5 archive. J. Adv. Model. Earth Syst. 6, 141–184. doi:10.1002/2013MS000265.
Steele, M., Morley, R., Ermold, W., 2001. PHC: a global ocean hydrography with a high quality arctic ocean. J. Clim. 14, 2079–2087.
Talley, L.D., Reid, J.L., Robbins, P.E., 2003. Data-based meridional overturning streamfunctions for the global ocean. J. Clim. 16, 3213–3226.
Toggweiler, J.R., Samuels, B., 1995. Effect of drake passage on the global thermohaline circulation. Deep-Sea Res. I 42, 477–500.
Toggweiler, J.R., Samuels, B., 1998. On the ocean's large-scale circulation near the limit of no vertical mixing. J. Phys. Oceanogr. 28, 1832–1852.
Wolfe, C.L., Cessi, P., 2010. What sets the strength of the middepth stratification and overturning circulation in eddying ocean models? J. Phys. Oceanogr. 40 (7), 1520–1538. doi:10.1175/2010JPO4393.1.
Wolfe, C.L., Cessi, P., 2014. Salt feedback in the adiabatic overturning circulation. J. Phys. Oceanogr. 44, 1175–1194. http://dx.doi.org/10.1175/JPO-D-13-0154.1.